Published in final edited form as:

Clin Cancer Res. 2019 July 15; 25(14): 4375–4387. doi:10.1158/1078-0432.CCR-18-4144.

PI3K/AKT/mTOR pathway alterations promote malignant progression and xenograft formation in oligodendroglial tumors

Kensuke Tateishi[1,2,13,14], **Taishi Nakamura**[1,14], **Tareq A. Juratli**[5,13], **Erik A. Williams**[3,13], **Yuko Matsushita**[2], **Shigeta Miyake**[1,14], **Mayuko Nishi**[6], **Julie J. Miller**[4,13], **Shilpa S. Tummala**[5,13], **Alexandria L. Fink**[5,13], **Nina Lelic**[5,13], **Mara V. A. Koerner**[5,13], **Yohei Miyake**[1,14], **Jo Sasame**[1,14], **Kenji Fujimoto**[2], **Takahiro Tanaka**[1], **Ryogo Minamimoto**[7], **Shigeo Matsunaga**[8], **Shigeo Mukaihara**[9], **Takashi Shuto**[1,8], **Hiroki Taguchi**[10], **Naoko Udaka**[11], **Hidetoshi Murata**[1], **Akihide Ryo**[6], **Shoji Yamanaka**[11], **William T. Curry**[5], **Dora Dias-Santagata**[3], **Tetsuya Yamamoto**[1], **Koichi Ichimura**[2], **Tracy T. Batchelor**[4,13], **Andrew S. Chi**[12,*], **A. John Iafrate**[3,13], **Hiroaki Wakimoto**[5,13], **Daniel P. Cahill**[5,13]

[1]Department of Neurosurgery, Yokohama City University Graduate School of Medicine, Yokohama, Japan.

[2]Division of Brain Tumor Translational Research, National Cancer Center Institute, Tokyo, Japan.

[3]Department of Pathology, Massachusetts General Hospital, Boston, MA.

[4]Stephen E. and Catherine Pappas Center for Neuro-Oncology, Department of Neurology, Massachusetts General Hospital Cancer Center, Harvard Medical School, Boston, Massachusetts, 02114, USA

[5]Department of Neurosurgery, Massachusetts General Hospital, Harvard Medical School, Boston, MA.

[6]Department of Microbiology, Yokohama City University Hospital, Yokohama, Japan.

[7]Division of Nuclear Medicine, Department of Radiology, National Center for Global Health and Medicine, Tokyo, Japan.

[8]Department of Neurosurgery, Yokohama Rosai Hospital, Yokohama, Japan.

[9]Department of Neurosurgery, Fujisawa Municipal Hospital, Fujisawa, Japan.

[10]Taguchi Neurosurgery Clinic, Department of Neurosurgery, Yokohama, Japan.

[11]Department of Pathology, Yokohama City University Hospital, Yokohama, Japan.

[12]Laura and Isaac Perlmutter Cancer Center, NYU Langone Medical Center, New York University, New York, NY.

Corresponding authors Kensuke Tateishi. M.D., Ph.D: ktate12@yokohama-cu.ac.jp; Hiroaki Wakimoto. M.D., Ph.D: hwakimoto@mgh.harvard.edu; Daniel P. Cahill M.D., Ph.D: cahill@mgh.harvard.edu.

*Present address: Neon Therapeutics, Cambridge, MA, USA

Disclosures:

A.J.I. has equity in ArcherDx and has received research support from Sanofi. T.T.B. has received research support from AstraZeneca, Pfizer, and Millennium, he is on the advisory board for UpToDate, Inc., and is a consultant for Champions Biotechnology, Genomicare, Merck, NXDC, Amgen, Roche, Oxigene, Foundation Medicine, Proximagen, he has provided CME lectures or material for Up To Date, Research to Practice, Oakstone Medical Publishing, and Imedex. A.S.C. is an employee of Neon Therapeutics. D.P.C. has received honoraria and travel reimbursement from Merck, and has served as a consultant for Lilly.

[13]Translational Neuro-Oncology Laboratory, Massachusetts General Hospital, Harvard Medical School, Boston, MA.

[14]Neurosurgical-Oncology Laboratory, Yokohama City University, Yokohama, Japan.

Abstract

Purpose: Oligodendroglioma (OD) has a relatively favorable prognosis, however, often undergoes malignant progression. We hypothesized that preclinical models of OD could facilitate identification of therapeutic targets in progressive OD. We established multiple OD xenografts to determine if PI3K/AKT/mTOR signaling pathway drives tumor progression.

Experimental Design: Two anatomically distinct tumor samples from a patient who developed progressive anaplastic oligodendroglioma (AOD), were collected for orthotopic transplantation in mice. We additionally implanted 13 tumors to investigate relationship between PI3K/AKT/mTOR pathway alterations and OD xenograft formation. Pharmacologic vulnerabilities were tested in newly developed AOD models *in vitro* and *in vivo*.

Results: A specimen from the tumor site that subsequently manifested rapid clinical progression contained a *PIK3CA* mutation E542K, and yielded propagating xenografts that retained the OD/AOD-defining genomic alterations (*IDH1*^{R132H} and 1p/19q co-deletion) and *PIK3CA*^{E542K}, and displayed characteristic sensitivity to alkylating chemotherapeutic agents. In contrast, a xenograft did not engraft from the region that was clinically stable and had wild-type *PIK3CA*. In our panel of OD/AOD xenografts, the presence of activating mutations in PI3K/AKT/mTOR pathway was consistently associated with xenograft establishment (6/6, 100%). OD/AOD that failed to generate xenografts did not have activating PI3K/AKT/mTOR alterations (0/9, $p<0.0001$). Importantly, mutant *PIK3CA* OD xenografts were vulnerable to PI3K/AKT/mTOR pathway inhibitors *in vitro* and *in vivo*, evidence that mutant *PIK3CA* is a tumorigenic driver in OD.

Conclusions: Activation of the PI3K/AKT/mTOR pathway is an oncogenic driver and is associated with xenograft formation in ODs. These findings have implications for therapeutic targeting of PI3K/AKT/mTOR pathway activation in progressive ODs.

Introduction

The World Health Organization (WHO) revised 2016 neuropathological classification defines oligodendroglioma (OD, grade II) and anaplastic oligodendroglioma (AOD, grade III) as a specific molecularly-defined subtype of adult diffuse gliomas. Mutation of the *isocitrate dehydrogenase* genes (*IDH½*) represents one of the fundamental and earliest molecular events in the genesis of these tumors (1,2), and has therefore been investigated as a potential therapeutic target (3-5). OD/AOD are also characterized by whole chromosome arm losses of 1p and 19q (6), and *TERT* promoter mutations are almost universal (>95%), while *CIC* and *FUBP1* are also frequently observed, irrespective of tumor grade (1,6-8). These molecular markers enabled improved classification of gliomas for predicting patient outcome (9,10). Additional recurring mutations, in the genes *PIK3CA*, *PIK3R1*, and *NOTCH1*, have been identified in a subset of oligodendroglial tumors (11-13). In contrast, *TP53* and *ATRX* mutations, which are commonly seen in astrocytic gliomas with *IDH*

mutation (diffuse astrocytoma, anaplastic astrocytoma, and secondary glioblastoma), are exceedingly rare in OD/AOD.

In aggregate, *IDH* mutant gliomas have better prognosis than *IDH* wild-type gliomas, across all WHO grades (12,14). Within *IDH* mutant gliomas, the prognosis of oligodendroglial (1p/19q codeleted) tumors is more favorable than astrocytic (*TP53* and *ATRX* mutated) tumors. Additionally, oligodendroglial tumors are highly responsive to radiation plus chemotherapy with procarbazine, lomustine (CCNU), and vincristine (known as PCV), or temozolomide (TMZ) (15-17). No survival difference could be distinguished between WHO grade II and grade III oligodendroglial tumors in a large clinical cohort (12). While ODs can undergo malignant degeneration with a fatal outcome (1,15-17), strict diagnostic reclassification by WHO 2016 raise the possibility that the progression of *IDH* mutant, 1p/19q co-deleted OD/AOD may be poorly characterized; indeed few studies have identified predictors of tumor progression within WHO2016-defined oligodendroglial tumors (11,18,19).

Recent studies have shown that, in OD/AOD, a subpopulation of undifferentiated cells was enriched for proliferative potential and expressed stem cell signature (20). This finding suggests that only a subset of undifferentiated cells plays a pivotal role in the maintenance of OD/AOD. Patient-derived glioma xenograft (PDX) models are derived from these undifferentiated cells, which manifest a cancer stem-like cell phenotype (21-23). Indeed, early-passage orthotopic xenografts generated with glioma tumorspheres, in most cases, recapitulate the phenotypic and genotypic characteristics of parent glioma, including critical driver gene mutations (24). Our recent efforts generating *IDH* mutant xenografts indicated that the establishment and propagation of these xenografts was often dependent upon the presence of a “tertiary” mutation (genomic alterations beyond disease-defining alterations in *IDH*, *ATRX*, *TP53*, and chromosomes 1p/19q), which was a hallmark of clinically-progressive behavior in the patient’s tumor (25). Given the indolent course of primary OD/AOD, it is therefore not surprising that establishment of tumor xenograft models has been difficult, with only a few models reported (5,26,27). Taken together, our experience suggests that focusing efforts on clinically-progressive OD/AOD may simultaneously achieve three important goals: 1) improving the chances of successful xenograft establishment, 2) providing insights into the genomic evolutionary events that underlies malignant progression in oligodendroglial tumors, and 3) identifying novel therapeutic targets for progressive tumors.

Herein, we describe a longitudinally monitored anaplastic oligodendroglioma (AOD) patient, who manifested progression of two anatomically separate tumors that were resected for investigation. From a region of the tumor that subsequently rapidly progressed, we successfully established patient-derived AOD xenografts. This xenograft harbored a hotspot mutation in *PIK3CA* and activation of the PI3K/AKT/mTOR pathway, findings that were also observed within this region of the patient’s tumor. In contrast, cells harvested from a distinct tumor region, which was stable after surgery and had wild-type *PIK3CA*, did not induce xenograft formation. Additional attempts at xenografting patient oligodendroglial tumors revealed a tight association between activating mutations in the *PI3K/AKT/mTOR*

signaling pathway and successful xenograft formation, supporting the pivotal role of PI3K/AKT/mTOR pathway in driving progression of oligodendroglial tumors.

Materials and methods

Creation of glioma tumorsphere lines, cell culture and reagents

This study was conducted in accordance with Declaration of Helsinki. All tumor and blood samples were collected with patient consent under protocols approved at Yokohama City University (YCU) Hospital and Massachusetts General Hospital (MGH) Institutional Review Boards. To create glioma tumorsphere lines, fresh tumor specimens were obtained from surgery and enzymatically dissociated with 0.1% of Trypsin and DNase. Tumorsphere lines were cultured in serum-free neural stem cell medium, as previously described (3,25,28). All tumorsphere lines were cryopreserved less than passage 3 to use for *in vitro* experiments. Temozolomide (TMZ, Sigma), Nimustine (ACNU, Tokyo Chemical Industry), Lomustine (CCNU), Procarbazine (Sigma), Vincristine (Sigma), FK866 (Sigma), LY294002 (Sellek), GDC-0068 (Cayman), BYL719 (Cayman), Everolimus (Cayman), and AGI-5198 (Sigma) were used.

Orthotopic xenograft model

$1–2\times10^5$ of cells were orthotopically implanted into the right striatum of 7–9-week-old female SCID Beige mice (Charles River, Yokohama or MA) within 24hrs after dissociation of tumor samples. Mice were monitored daily and sacrificed when neurologic deficits or general condition reached the criteria for euthanasia. Brains were harvested for pathological studies and for acutely dissociated tumor cells that were cryopreserved, cultured for *in vitro* experiments, or repeatedly implanted into mice brains. All mouse experiments were approved by the Institutional Animal Care and Use Committee at MGH and YCU.

Histology and immunohistochemistry

Tumor tissue specimens were fixed in 10% neutral-buffered formalin and embedded in paraffin. Hematoxylin and eosin staining was performed using the standard procedures. For immunohistochemistry (IHC), 5 μm thick sections were deparaffinized, treated with 0.5% H_2O_2 in methanol, rehydrated, and heated for 20 minutes of antigen retrieval. After blocking with serum, tissue sections were incubated with primary antibody (1:100 for $IDH1^{R132H}$ (Dianova), Ki-67 (Dako), MSH6 (Proteintech), LKB1/STK11 (Novus Biologicals), p-AKT (Ser473, Cell Signaling Technology (CST)), p-4EBP1 (CST), p-S6K (CST), p-S6 ribosomal protein (CST), ATRX (Sigma), p53 (Leica), p16INK4a/CDKN2A (R&D) at 4°C overnight. The next day, sections were washed with PBS, incubated with biotinylated secondary antibody for 30 minutes at room temperature, then incubated with ABC solution (PK-6101, PK-6102; Vector laboratories) for 30 minutes at room temperature. Finally, sections were incubated with DAB (Dako) and counter-stained with hematoxylin. Only strongly stained cells were considered positive. Positive stained cells were quantitatively analyzed and classified as strong (≧20%), moderate (5–20%), and weak (≦5%), respectively.

Western blotting

Cells were then lysed in RIPA buffer (Sigma-Aldrich) with a Protease Inhibitor Cocktail Tablets (Roche). 50μg of protein was separated by 10% SDS-PAGE and transferred to polyvinylidene difluoride membranes (Millipore) by electroblotting. After blocking with 1 or 5% nonfat dry milk in TBST (25 mM Tris [pH, 7.4], 137 mM NaCl, 0.5% Tween20), membranes were incubated at 4C overnight with primary antibodies. After washing and incubation with horseradish peroxidase-conjugated secondary antibodies (CST), blots were washed, and signals were visualized with chemiluminescent HRP substrate (Millipore). Primary antibodies used were: p-AKT, p-mTOR (CST), p-4EBP1, p-S6K, Actin (CST) and Vinculin (CST).

Molecular analysis

Genomic and bisulfite-modified DNA was extracted using DNeasy Blood & Tissue and EpiTect Bisulfite kits (Qiagen), per manufacture's protocol. PCR protocol and primer sequencing for *IDH1* (exon 4), *IDH2* (exon 4), *TERT* promoter, *STK11* (exon 6), and *PIK3CA* (exons 8, 9, and 20) are described in Supplementary Table 1. Methods for cell line fingerprinting, Sanger Sequencing, Pyrosequencing, FISH, MLPA, multiplex PCR technology (SNaPShot), and microsatellite instability analysis are described in Supplementary methods.

Cell Viability Analysis

To assess cell viability, tumorspheres were dissociated into single cells and seeded into 96-well plates at 7,000–8,000 cells/well. After 12–24 hours, chemical inhibitors were serially diluted and added to wells. Cell viability was measured by CellTiter-Glo (Promega) assay at indicated time points.

^{11}C-Methionine positron emission tomography (PET) imaging

Methionine (MET)-PET CT was performed at National Center for Global Health and Medicine (Tokyo), as previously described (29). For semiquantitative interpretations, the standardized uptake value (SUV) max was determined by a standard formula. The tumor/normal ratio (T/N ratio) of MET was calculated relative to the uptake in the contralateral frontal cortex.

Statistical Analysis

Statistical analysis was performed with JMP Pro12 software (Cary, NC). For parametric analysis, two-tailed t tests were used. Two-tailed Fisher exact test was performed for analysis of frequencies of nominal data. Survival analysis was performed using Kaplan-Meier method, and log-rank test was used to compare survival differences. Data were expressed as mean ± SEM. $P < .05$ was considered statistically significant.

Results

Case presentation

The clinical course and pathological findings of a representative patient (YMG6) are shown (Fig. 1A, Supplementary Fig. S1A), and summarized briefly as follows: A previously healthy 33-year-old man presented with headache and magnetic resonance imaging (MRI) of the brain revealed a non-contrast enhancing cystic lesion located within the left frontal lobe. This primary tumor (designated YMG6I) underwent radiographically-complete resection and was diagnosed as AOD, with 20% of Ki-67 positive cells. The patient then underwent 60 Gy of radiotherapy as an adjuvant treatment. Nine years later, MRI revealed a small non-contrast enhancing lesion at the margin of the original tumor site. ^{11}C-methionine PET imaging, which has utility for evaluating recurrent gliomas (30), revealed a relatively high uptake (Fig. 1A), consistent with tumor recurrence. The recurrent tumor was resected and the pathological diagnosis was WHO grade II glioma (YMG6R1) consisting of reactive astrocytes admixed with atypical cells. TMZ was administered for 24 cycles. Four years later, a contrast enhanced recurrent lesion emerged, that was again resected (YMG6R2) and the diagnosis was AOD (WHO grade III). TMZ treatment resumed for additional 20 cycles. However, two distant contrast-enhancing tumors with higher uptake of ^{11}C-methionine developed: one at the left frontal base (YMG6R3F) and a second within the left medial temporal lobe (YMG6R3T), while the initial site of tumor remained unchanged. Gross total resection was performed for both distant tumors. Both tumors were diagnosed as WHO grade III glioma with Ki-67 index approximately 40%. Intriguingly, YMG6R3T (left temporal tumor) subsequently developed a rapid local recurrence in 4 months, while the left frontal tumor (YMG6R3F) has remained stable for more than 24 months. Finally, the left temporal tumor was again resected (YMG6R4) with the histopathology exhibiting similar findings (WHO grade III).

Genomic analysis identified mutations in *IDH1* (R132H) and the *TERT* promoter (c. −124C>T, C228T) in all the tumors throughout the course including the initial tumor (YMG6I), consistent with these mutations being early events in gliomagenesis (1,11,12) (Figure 1B, Supplementary Fig. S1B). Fluorescent in situ hybridization (FISH) and Multiplex ligation-dependent probe amplification (MLPA) assay demonstrated whole chromosome arm losses of 1p and 19q (Fig. 1B, Supplementary Fig. S1B and C). Altogether, the WHO 2016 integrated classification was AOD, *IDH1* mutant and 1p/19q co-deleted.

PIK3CA mutation activating PI3K/AKT/mTOR pathway in anaplastic oliogodendroglioma

We confirmed matched DNA identification in YMG6R3F and YMG6R3T cells (Supplementary Fig. S2. To evaluate genomic evolution, we profiled each tumor using an NGS panel that interrogates the exons of 94 cancer-related genes, direct DNA sequencing, and immunohistochemical analysis (Fig. 1C, Supplementary Figure S1B, Supplementary Table 2). We found sequence variants in *MSH6* and *STK11* in normal blood DNA, not previously reported as pathogenic mutations, likely indicating germline polymorphisms (Supplementary Table 2, Supplementary Fig. S3A). MSH6 and STK11 was positively expressed in YMG6I (Supplementary Figs. S3B-C). Germline mutations in the *MSH6* and

STK11 are associated with Lynch syndrome and Peutz-Jeghers Syndrome, respectively. However, upper gastrointestinal endoscopy, endoscopy colonoscopy, and whole body FDG-PET imaging did not find any findings to suggest these diagnoses were present in this patient (Supplementary Figs. S3E-G). Additionally, MSI was not found in all tumor samples, including non-hypermutant YMG6R2 and hypermutant YMG6R3T (Supplementary Fig. S4, Supplementary Table 3), further evidence against these germline mutations directly promoting AOD growth or treatment resistance in this case.

Five mutations were detected in YMG6R2 (*IDH1*, *TERT*, *MSH6*, *STK11*, and *SMARCA4*), while tumor specimens from subsequent recurrences harbored a much greater number of mutations: YMG6R3F (29 mutations), YMG6R3T (55), and YMG6R4T (27) cells, respectively (Fig. 1C). Twenty-seven of 29 (93.1%) mutations in YMG6R3F were shared by YMG6R3T, while 28 of 55 (50.9%) YMG6R3T mutations were private. YMG6R4T had all the 27 mutations that YMG6R3F and YMG6R3T shared but did not have the 2 private mutations of YMG6R3F (Fig. 1C, Supplementary Table 2). These findings imply that YMG6R3T and YMG6R4T arose from a subclone of YMG6R3F, and subsequently acquired additional mutations.

The elevated number of mutations in YMG6R3F, YMG6R3T, and YMG6R4T were suggestive of the emergence of a DNA hypermutation phenotype. G:C>A:T transition mutations were overwhelmingly dominant, as observed in 28/29 (96.6%) in YMG6R3F, 51/55 (92.7%) in YMG6R3T, and 26/27 (96.3%) in YMG6R4T, a pattern consistent with TMZ-associated DNA hypermutation (1,31) (Fig. 1D). We then focused on mutations other than the 5 detected in the low-mutant load YMG6R2. Considering the strand on which C>T change occurred, the majority of C>T changes were observed at non-CpG sites, a signature of TMZ-associated mutation rather than spontaneous deamination, as mutations at CpG sites were only 16.0%, 13.3%, and 19.0% in YMG6R3F, YMG6R3T, and YMG6R4T, respectively (Fig. 1E). Somatic mutation of $MSH6^{Gly409Glu}$ was identified in YMG6R4T in which MSH6 expression was negative (Supplementary Figs. S3B and 3D). Thus, the DNA hypermutation phenotype of these later recurrences was consistent with TMZ treatment induced hypermutation, manifest in this case after at least 24 cycles of TMZ treatment. Recurrent glioma with TMZ-associated hypermutation has been shown to have increased *MGMT* methylation compared to initial untreated tumors (32). In the present case, both non-hypermutated and hypermutated tumors after TMZ treatment had high *MGMT* promoter methylation status (Supplementary Table 4).

Of note, among the 28 private mutations of YMG6R3T, only *PIK3CA* (c.1624G>A, Glu542Lys) was retained in YMG6R4T (Fig. 1C and F, Supplementary Table 2), an observation suggesting $PIK3CA^{E542K}$, and not the other private mutations, may be a driver genetic event of YMG6R3T and YMG6R4T. Interpreting the functional consequences of individual mutations in cases with hypermutation can be difficult, as the vast majority of alterations are non-selected passenger events (1). Nonetheless, *PIK3CA* mutations at highly recurrent sites (E542K, E545K, and H1047R) have been shown to activate oncogenic PIK3/AKT/mTOR pathways in cancer (33,34). By contrast, mutations in *ATRX* and *TP53* were identified in YMG6R3T, not YMG6R4T, and IHC analysis demonstrated retained expression of ATRX and low expression of p53 in YMG6R3T (Supplementary Fig. S5),

indicating these may be non-functional passenger mutations. Intriguingly, pyrosequencing identified *PIK3CA*^{E542K} mutation in a small subset of tumor cells in YMG6I, which during subsequent treatment then fell below the detection limit in YMG6R1, YMG6R2, and YMG6R3F (Supplementary Fig. S6A). No other PI3K/AKT/mTOR pathway gene mutation was identified in YMG6R2 and YMG6R3F (Fig. 1C and F, Supplementary Table 2). To assess the functional consequences of *PIK3CA*^{E542K} mutation, we performed IHC for downstream effectors in the PI3K/AKT/mTOR pathway. Results demonstrated strong expression of p-AKT as well as p-4EBP1 and p-S6K, in YMG6R3T and YMG6R4T, but not in YMG6R1, YMG6R2, and YMG6R3F (Fig. 1G, Supplementary Fig. S6B). We did note scattered expression of p-4EBP1 and p-S6K in YMG6I, consistent with PI3K/AKT/mTOR pathway activation in a subset of cells with *PIK3CA*^{E542K}.

Orthotopic anaplastic oligodendroglioma xenograft models recapitulate patient phenotypic and genotypic features

Glioma sphere cell lines were established from YMG6R3F and YMG6R3T and implanted into mice brains to assess the potential for engraftment. YMG6R3F implanted mice did not develop neurological symptoms during a 250-day follow-up period and autopsy revealed only a small tumor (YMG6R3F secondary cells, derived from 1st generation xenograft, designated YMG6R3Fsc, Fig. 2A). In contrast, YMG6R3T implanted mice rapidly developed neurologic deterioration (124 days), and large nodular tumors expressing IDH1^{R132H} were found (YMG6R3Tsc, Fig. 2B). Histologically, glial tumor cells with atypical nuclei that resembling oligodendrocytes exhibited high proliferative activity (Ki-67 index of 40%), consistent with the diagnosis of AOD (Fig. 2C). For genomic analysis, we first confirmed matched DNA identification between YMG6RT3 and the first generation xenograft YMG6R3Tsc1 (Supplementary Fig. S2). YMG6R3Tsc1 harbored mutations in *IDH1* (R132H) and *TERT* promoter (c.−124C>T, C228T), and whole chromosome arm loss of 1p and 19q (Fig. 2D and E, Supplementary Figure S7A), fulfilling the WHO 2016 diagnostic criteria of oligodendroglioma. YMG6R4T cells were also tumorigenic (YMG6R4Tsc, Fig. 2F and G), and recapitulated the genotype of AOD (Supplementary Fig. S7B). After serial transplantation in mouse brains, PDXs generated from YMG6R3T and YMG6R4T cells maintained the phenotypic and genotypic characteristics of AOD (Supplementary Fig. S8A-C). YMG6R3T and YMG6R4T xenografts were similarly and consistently lethal within 130 days whereas YMG6R3F xenografts did not cause animal death (Fig. 2H).

PI3K/AKT/mTOR pathway gene mutation is tightly associated with anaplastic oligodendroglioma orthotopic xenograft formation

We identified 15 mutations in YMG6R3Tsc1 xenografts (Fig. 2I, Supplementary Table 2). Among them, 8 mutations, including *IDH1*^{R132H}, *TERT* promoter, *PIK3CA*^{E542K}, were retained from the parental primary tumor (YMG6R3T). Interestingly, we identified only 5 mutations in YMG6R4Tsc1, derived from the tumor that progressed after YMG6R3T, including *IDH1*^{R132H}, *TERT* promoter, and *PIK3CA*^{E542K} (Fig. 2I, Supplementary Table 2), whereas the other mutations (associated with hypermutation phenotype) that were lost were passengers. Importantly, we confirmed the maintenance of *PIK3CA*^{E542K} in serially passaged xenografts by Sanger sequencing (Fig. 2J, Supplementary Fig. S8C). IHC analysis

revealed strong expression of p-AKT, p-4EBP1, and p-S6K in YMG6R3T and YMG6R4T xenografts, as compared to non-lethal, slow-growing YMG6R3F xenografts (Fig. 2K, Supplementary Fig. S8D). We therefore hypothesized that *PIK3CA*^{E542K} is the driver mutation that promotes OD progression in the patient and in orthotopic xenografts.

To test the hypothesis that genetic activation of the PI3K/AKT/mTOR pathway promotes xenograft formation in oligodendroglial tumors, we collected 12 additional OD specimens that harbored mutations in *IDH1*^{R132H} and the *TERT* promoter, and 1p/19q co-deletion, and performed orthotopic transplantation assays (Table 1). This cohort included 4 AODs with NGS-detected genetic alteration in the PI3K/AKT/mTOR pathway (Supplementary Table 5): YMG23 (newly diagnosed AOD, *PIK3CA*^{His1047Arg} and *CDKN2A-CDKN2B* homozygous deletion, Fig. 3A, Supplementary Fig. S9A-B); YMG5 (recurrent AOD, *PIK3R1*^{Ile571AsnfsTer31}, Fig. 3B, Supplementary Fig. S9C); MGG60 (newly diagnosed AOD, *PIK3CA*^{His1047Leu})(25); MGG137 (newly diagnosed AOD, *MTOR*^{Ser2215Phe}, Fig.3C). We observed xenograft formation from YMG5, YMG23, MGG60, and MGG137, which all harbored genetic alteration in the PI3K/AKT/mTOR pathway (Fig. 3D-F). Mutations of *IDH1*, *TERT*, and *PIK3CA* as well as *CDKN2A-CDKN2B* homozygous deletion and p16INK4a/CDKN2A inactivation were retained in YMG23sc1 xenografts (Supplementary Fig. S9D-F). In contrast, we did not observe xenograft formation from YMG46, which harbored alteration of *PIK3CA*^{Glu469Gly}, not reported in the COSMIC database (Fig. 3G-H, Supplementary Fig. S10A, Supplementary Table 5). Also, we did not detect PI3K/AKT/mTOR pathway mutation in seven ODs/AODs: YMG28, YMG53, MGG78, MGG82, MGG109, MGG126, and MGG130 (Table 1, Fig. 3I-J, Supplementary Fig. S10B-C) (25). These ODs/AODs without activating PI3K/AKT/mTOR pathway alteration did not form orthotopic xenografts (Table 1, Figure 3I-J, Supplementary Fig. S10D). Presence of PI3K/AKT/mTOR pathway gene activating mutation was therefore tightly associated with xenograft lethality (6/6 PI3K/AKT/mTOR pathway mutant vs. 0/9 PI3K/AKT/mTOR pathway wildtype; P<.0001, Table 1, Fig. 3K). There was no significant difference in Ki-67 index between xenograft generating and non-generating patient specimens (P = 0.13, Supplementary Table 6).

Immunohistochemistry of patient tumor specimens demonstrated detectable expression of p-AKT, p-4EBP1 and p-S6K (or p-S6) in PI3K/AKT/mTOR pathway-mutated YMG23, YMG5, and MGG137 (Fig. 4A-C, Supplementary Table 6), as opposed to weak expression in PI3K/AKT/mTOR pathway-wild-type YMG28, YMG46, and YMG53 (Fig. 4D-F). The xenografts derived from AODs carrying activating alterations in PI3K/AKT/mTOR pathway similarly recapitulated increased expression of p-4EBP1 and p-S6K or p-S6 (Fig. 4A-C, Supplementary Table 7). Phosphorylation of AKT was also preserved in *PIK3CA*-mutant xenografts, YMG23sc1 and YMG5sc1. Serially passaged xenografts of YMG23 retained mutations of *IDH1*, *TERT*, and *PIK3CA* as well as PI3K/AKT/mTOR pathway activation found in the patient (Supplementary Fig. S11). Taken together, our results support a proposed role for activating PIK3/AKT/mTOR pathway alterations in promoting tumor progression and xenograft formation in oligodendroglial tumors.

Therapeutic vulnerability of PI3K pathway activated anaplastic oligodendroglioma

The YMG6 patient experienced tumor progression on prolonged TMZ therapy, suggestive of emergence of acquired resistance (Figure 1A). Our PDX models offered an opportunity to test therapeutic vulnerabilities *in vitro* and *in vivo*. We first used a cell viability assay to test TMZ response of tumor neurosphere cultures (tumorspheres) derived from the patient tumor *in vitro*. Despite methylated MGMT promoter, *MSH6* inactivated YMG6R4T cells were highly resistant to TMZ, in line with reported effects of mismatch repair deficiency on TMZ response (Fig. 5A, Supplementary Fig. S3D, Supplementary Table 2) (35,36). YMG23 (AOD, *MGMT* unmethylated) and YMG14 (GBM, *IDH* wild-type, *MGMT* unmethylated) tumorspheres were also resistant to TMZ, while YMG12 (GBM, *IDH* wild-type, *MGMT* methylated, MMR intact) and MGG152 (GBM, *IDH1* mutant, *MGMT* methylated, MMR intact) tumorspheres were responsive. Indeed, YMG23 and YMG14 patient tumors progressed on TMZ (Supplementary Fig. S12A-B). These results support the proposal that either inactivated MSH6 or unmethylated *MGMT* promoter can increase TMZ resistance in glioma.

Intriguingly, in patient YMG6, a progressive contrast enhancing lesion that emerged after removal of YMG6R4T showed complete response to 4 cycles of procarbazine, nimustine (ACNU), and vincristine, the regimen called “PAV”, which is analogous to PCV (Fig. 5B). Consistent with this clinical observation, YMG6R4T tumorspheres also responded to ACNU, CCNU, procarbazine, and vincristine (monotherapy) *in vitro* (Fig. 5C). YMG23 cells also responded to ACNU, CCNU, and procarbazine, but resisted vincristine. In contrast, YMG36 (GBM, *IDH*-wild type) responded rather poorly to ACNU, CCNU and vincristine (Fig. 5C). Clinically, PIK3/AKT/mTOR gene mutant tumors, YMG5 and MGG137, showed durable response to chemotherapeutic agents (PAV or TMZ regimen) (Supplementary Fig. 12C and D). These observations indicate that alkylating agents can still retain effectiveness in PIK3/AKT/mTOR pathway mutant ODs, suggesting instead that alkylator sensitivity is dependent on MMR status or *MGMT* promoter status (37). Indeed, we did not find significant differences between the overall survival of patients with *PIK3CA/PIK3R1* mutant ODs as compared with patients with *PIK3CA/PIK3R1* wild-type ODs (Supplementary Fig. S13, Supplementary Table 8).

We recently reported that metabolic depletion of NAD+ using NAMPT inhibitors alone or in combination with TMZ, which also lowers intracellular NAD+ levels, represents a potential therapeutic strategy for *IDH1* mutant gliomas (3,35,38). As expected, OD/AOD tumorspheres were sensitive to NAMPT inhibitor, and combination with TMZ increased the NAMPT inhibitor effects (Fig. 5D, Supplementary Fig. S14A). On the other hand, OD/AOD tumorspheres were resistant to direct inhibition of the mutant IDH1 enzyme using AGI-5198 (Fig. 5E, Supplementary Fig. S14B), consistent with previous observations in gliomaspheres (3).

We next tested if inhibition of PI3K-AKT-mTOR signaling could inhibit xenograft formation and induce selective cytotoxicity in PI3K pathway altered AOD. To test if inhibitors of the PI3K pathway could suppress PI3K/AKT/mTOR pathway, YMG6R4T xenograft cells were treated with DMSO, 50 μM of LY294002, or 5 μM of GDC-0068 for 12 hrs. As expected, PI3K inhibitor LY294002 and AKT inhibitor GDC-0068 potently blocked phosphorylation

of AKT, mTOR, 4EBP1, and S6K in YMG6R4T cells (Fig. 5F), indicating on-target effects. We treated YMG6R4T cells with DMSO or LY294002 for 24hr *in vitro*, and implanted them orthotopically. LY294002 and GDC-0068 induced cytotoxic effects in *PIK3CA*-mutant YMG6R4T and YMG23 cells while they did not in *PIK3CA* wild-type YMG28 tumorsphere cells and (Fig. 5G). A similar profile was observed when YMG6R4T and YMG23 (PIK3/AKT/mTOR pathway mutant; sensitive) and YMG28 (resistant) were tested with another PI3K inhibitor (BYL719) and an mTOR inhibitor (everolimus) (Fig. 5H). By contrast, YMG46 (non-activating mutation of *PIK3CA(E469K*) was not sensitive to these compounds (Fig. 5I). Finally, we confirmed LY294002 treatment, compared to DMSO, potently suppressed the lethal progression of YMG6R4T cells *in vivo* (Fig. 5J). Together, these results suggest that activating mutations in the PIK3/AKT/mTOR pathway may predict response to targeted inhibition of this signaling pathway.

Discussion

PI3K pathway genes are frequently mutated in oligodendroglial tumors, including *PIK3CA* (20%) and *PIK3R1* (9%) (13). These mutations are predominantly found in recurrent tumors when paired primary and progressive tumors are compared (11), implying acquisition of PI3K pathway mutation is associated with progression, and therefore may be a driver for malignant transformation. However, beyond these temporal associations, no evidence exists supporting these mutations as promoters of tumor progression in OD. We here provide functional evidence that PIK3/AKT/mTOR pathway activating mutation promotes malignant progression using a series of patient-intracranial oligodendroglial xenografts and a patient whose two evolutionarily divergent and genetically distinct tumors followed contrasting clinical and laboratory courses. In the patient case, the $PIK3CA^{E542K}$ mutant tumor rapidly recurred and formed lethal xenografts, while the *PIK3CA* wild-type tumor did not progress nor form progressive xenografts. In our oligodendroglioma series, we found that hotspot mutation and activation of the PI3K/AKT/mTOR pathway was tightly associated with progressive AOD xenografts, and found that PI3K/AKT/mTOR pathway activated mutant tumor models were selectively sensitive to PI3K/AKT/mTOR pathway inhibitors.

PI3K/AKT/mTOR pathway is a canonical growth regulatory pathway in cancer. A pan-cancer proteo-genomic atlas demonstrated that PI3K/AKT/mTOR pathway activation was correlated with distribution of mutations in key PI3K/AKT/mTOR pathway genes (33). Highly recurrent mutations at E542, E545, and H1047 in *PIK3CA*, nonsense/frameshift/indel mutations involving *PIK3R1*, and hotspot mutation (e.g. S2215F) in *MTOR* all potently induced expression of p-AKT (Ser473). In contrast, tumors with mutations not predicted to be functional demonstrated weak or no significant effect on p-AKT (Ser473) (33). These prior reports, alongside our current work, collectively support the model that alterations in PI3K/AKT/mTOR pathway genes activate the PI3K pathway and promote malignant progression in oligodendroglial tumors.

Previous reports indicate that recurrence of OD is not accompanied by dramatic changes in the number of mutation and genome-wide methylation status (39). Interestingly, our case study displayed DNA hypermutation after tumor progression on TMZ, and *PIK3CA* mutation emerged in one of the two recurrent lesions. Notably however, both *PIK3CA*

mutant (YMG6R3T) and *PIK3CA* wild-type (YMG6R3F) tumors harbored a DNA hypermutation phenotype, yet the former subsequently progressed and the latter did not, indicating the DNA hypermutation phenotype itself was not a direct promoter of malignant progression. In addition, the fact that the DNA hypermutation phenotype was lost in the subsequent progressive tumor (YMG6R4T) suggests the majority of mutations found in YMG6R3T might be passengers, whereas serially retained mutations, such as $PIK3CA^{E542K}$, represent the functional drivers.

As few OD xenograft models have been established to date, complete knowledge of the molecular drivers of OD progression remain unclear (5,26,27). A previous study demonstrated that ectopic expression of $IDH1^{R132H}$ in the subventricular zone of the mouse brain induced early *IDH* mutant gliomagenesis, including 2-hydroxyglutarate production and a global DNA methylation phenotype, however, was unable to sustain tumor growth (40). We also reported that secondary mutations, including *TP53* and *ATRX* in astrocytic tumors or *TERT* promoter mutation and 1p/19q co-deletion in OD, were not sufficient to form *IDH1* mutant xenografts in immunocompromised mice (25). Recently, Philip *et al.* demonstrated mutant *IDH1* cooperated with *PDGFRA* and loss of *CDKN2A*, *ATRX*, and *PTEN* to promote tumor development *in vivo* (41). These findings suggest that a tertiary genomic event may be required for xenograft formation in ODs as well.

All of our progressive OD xenograft models that successfully generated orthotopic xenograft carried functional genetic alterations in *PIK3CA*, *PIK3R1*, or *MTOR*. In contrast, none of PI3K pathway gene wild-type tumors or tumor with *PIK3CA* non-functional mutation induced xenograft formation. Clinically, we observed rapid tumor progression after resection of YMG6R3T and YMG6R4T (*PIK3CA* mutant), whereas YMG6R3F (*PIK3CA* wild-type) remained stable post-operatively, mirroring the inability to generate xenograft *ex vivo*. These findings are consistent with previous studies that associated genomic alterations in the PI3K pathway, such as *PIK3CA* and *PIK3R1* mutations, with progression in *IDH1* mutant gliomas (11,25). A recent study also demonstrated that hotspot mutations in *PIK3CA* potentiated PI3K signaling and promoted tumorigenesis of immortalized normal human astrocytes *in vivo* (42). In support of these findings, our study also demonstrated delayed xenograft growth by PI3K pathway inhibition. These results support the crucial role of PI3K/AKT/mTOR pathway gene alteration in the formation and progression of OD xenografts.

Our OD xenograft models should facilitate research exploring therapeutic targets in progressive oligodendroglial tumors. Using these models, we provide experimental evidence that oligodendroglial tumors with PI3K/AKT/mTOR mutation are susceptible to selective inhibition of the PI3K/AKT/mTOR pathway. Interestingly, alkylating chemotherapeutics such as ACNU and procarbazine remained effective in the patients described and our OD models after developing resistance to TMZ and developing TMZ-induced hypermutation phenotype. Indeed, we did not find a survival difference of *PIK3CA/PIK3R1* mutant ODs, when compared with wild-type ODs. Also, we found in our index case, that although the primary tumor (YMG6I) harbored $PIK3CA^{E542K}$, this subpopulation of cells fell below the limit of detection during radiation and temozolomide treatment. These findings imply that PI3K pathway gene alteration in ODs may promote malignant progression, but not necessarily resistance to effective cytotoxic chemotherapies. Early detection of subclonal

PI3K pathway activating mutations could therefore potentially inform the timing of initiating such treatments, although further translational clinical studies will be needed to guide treatment decisions for OD patients.

In conclusion, we identified the critical role of PI3K/AKT/mTOR gene activating mutation in promoting malignant transformation and generating xenografts in oligodendroglial tumors. These xenograft models provide insights into potential therapeutic targets, including PI3K/AKT/mTOR pathway inhibitors, in a subset of oligodendroglial tumors.

Supplementary Material

Refer to Web version on PubMed Central for supplementary material.

Acknowledgements

The authors thank Mrs. Emi Hirata and Yasuko Tanaka for technical assistance.

Grant support

This work was supported by Grant-Aid for Scientific Research C (16K10765 to KT), Princess Takamatsu Cancer Research Fund (KT), Takeda Science Foundation (KT), The Yasuda Medical Foundation (KT), Japanese Foundation for Multidisciplinary Treatment of Cancer (KT), Yokohama Foundation for Advancement of Medical Science (KT), SGH Foundation for Cancer Research (KT), Bristol-Myers Squibb Research grant (KT), OligoNation (DPC), and NIH R01CA227821 (to DPC and HW).

References

1. Johnson BE, Mazor T, Hong C, Barnes M, Aihara K, McLean CY, et al. Mutational analysis reveals the origin and therapy-driven evolution of recurrent glioma. Science 2014;343(6167):189–93 doi 10.1126/science.1239947. [PubMed: 24336570]
2. Yan H, Parsons DW, Jin G, McLendon R, Rasheed BA, Yuan W, et al. IDH1 and IDH2 mutations in gliomas. N Engl J Med 2009;360(8):765–73 doi 10.1056/NEJMoa0808710. [PubMed: 19228619]
3. Tateishi K, Wakimoto H, Iafrate AJ, Tanaka S, Loebel F, Lelic N, et al. Extreme Vulnerability of IDH1 Mutant Cancers to NAD+ Depletion. Cancer Cell 2015;28(6):773–84 doi 10.1016/j.ccell.2015.11.006. [PubMed: 26678339]
4. Schumacher T, Bunse L, Pusch S, Sahm F, Wiestler B, Quandt J, et al. A vaccine targeting mutant IDH1 induces antitumour immunity. Nature 2014;512(7514):324–7 doi 10.1038/nature13387. [PubMed: 25043048]
5. Rohle D, Popovici-Muller J, Palaskas N, Turcan S, Grommes C, Campos C, et al. An inhibitor of mutant IDH1 delays growth and promotes differentiation of glioma cells. Science 2013;340(6132):626–30 doi 10.1126/science.1236062. [PubMed: 23558169]
6. Killela PJ, Reitman ZJ, Jiao Y, Bettegowda C, Agrawal N, Diaz LA, Jr., et al. TERT promoter mutations occur frequently in gliomas and a subset of tumors derived from cells with low rates of self-renewal. Proc Natl Acad Sci U S A 2013;110(15):6021–6 doi 10.1073/pnas.1303607110. [PubMed: 23530248]
7. Arita H, Narita Y, Fukushima S, Tateishi K, Matsushita Y, Yoshida A, et al. Upregulating mutations in the TERT promoter commonly occur in adult malignant gliomas and are strongly associated with total 1p19q loss. Acta Neuropathol 2013;126(2):267–76 doi 10.1007/s00401-013-1141-6. [PubMed: 23764841]
8. Bettegowda C, Agrawal N, Jiao Y, Sausen M, Wood LD, Hruban RH, et al. Mutations in CIC and FUBP1 contribute to human oligodendroglioma. Science 2011;333(6048):1453–5 doi 10.1126/science.1210557. [PubMed: 21817013]
9. Arita H, Yamasaki K, Matsushita Y, Nakamura T, Shimokawa A, Takami H, et al. A combination of TERT promoter mutation and MGMT methylation status predicts clinically relevant subgroups of

newly diagnosed glioblastomas. Acta Neuropathol Commun 2016;4(1):79 doi 10.1186/s40478-016-0351-2. [PubMed: 27503138]

10. Eckel-Passow JE, Lachance DH, Molinaro AM, Walsh KM, Decker PA, Sicotte H, et al. Glioma Groups Based on 1p/19q, IDH, and TERT Promoter Mutations in Tumors. N Engl J Med 2015;372(26):2499–508 doi 10.1056/NEJMoa1407279. [PubMed: 26061753]
11. Bai H, Harmanci AS, Erson-Omay EZ, Li J, Coskun S, Simon M, et al. Integrated genomic characterization of IDH1-mutant glioma malignant progression. Nat Genet 2016;48(1):59–66 doi 10.1038/ng.3457. [PubMed: 26618343]
12. Suzuki H, Aoki K, Chiba K, Sato Y, Shiozawa Y, Shiraishi Y, et al. Mutational landscape and clonal architecture in grade II and III gliomas. Nat Genet 2015;47(5):458–68 doi 10.1038/ng.3273. [PubMed: 25848751]
13. Cancer Genome Atlas Research N, Brat DJ, Verhaak RG, Aldape KD, Yung WK, Salama SR, et al. Comprehensive, Integrative Genomic Analysis of Diffuse Lower-Grade Gliomas. N Engl J Med 2015;372(26):2481–98 doi 10.1056/NEJMoa1402121. [PubMed: 26061751]
14. van den Bent MJ, Smits M, Kros JM, Chang SM. Diffuse Infiltrating Oligodendroglioma and Astrocytoma. J Clin Oncol 2017;35(21):2394–401 doi 10.1200/JCO.2017.72.6737. [PubMed: 28640702]
15. Buckner JC, Shaw EG, Pugh SL, Chakravarti A, Gilbert MR, Barger GR, et al. Radiation plus Procarbazine, CCNU, and Vincristine in Low-Grade Glioma. N Engl J Med 2016;374(14):1344–55 doi 10.1056/NEJMoa1500925. [PubMed: 27050206]
16. van den Bent MJ, Taphoorn MJ, Brandes AA, Menten J, Stupp R, Frenay M, et al. Phase II study of first-line chemotherapy with temozolomide in recurrent oligodendroglial tumors: the European Organization for Research and Treatment of Cancer Brain Tumor Group Study 26971. J Clin Oncol 2003;21(13):2525–8 doi 10.1200/JCO.2003.12.015. [PubMed: 12829671]
17. Cairncross JG, Ueki K, Zlatescu MC, Lisle DK, Finkelstein DM, Hammond RR, et al. Specific genetic predictors of chemotherapeutic response and survival in patients with anaplastic oligodendrogliomas. J Natl Cancer Inst 1998;90(19):1473–9. [PubMed: 9776413]
18. Halani SH, Yousefi S, Vega JV, Rossi MR, Zhao Z, Amrollahi F, et al. Multi-faceted computational assessment of risk and progression in oligodendroglioma implicates NOTCH and PI3K pathways. NPJ Precis Oncol 2018;2:24 doi 10.1038/s41698-018-0067-9. [PubMed: 30417117]
19. Aoki K, Nakamura H, Suzuki H, Matsuo K, Kataoka K, Shimamura T, et al. Prognostic relevance of genetic alterations in diffuse lower-grade gliomas. Neuro Oncol 2018;20(1):66–77 doi 10.1093/neuonc/nox132. [PubMed: 29016839]
20. Tirosh I, Venteicher AS, Hebert C, Escalante LE, Patel AP, Yizhak K, et al. Single-cell RNA-seq supports a developmental hierarchy in human oligodendroglioma. Nature 2016 doi 10.1038/nature20123.
21. Luchman HA, Stechishin OD, Dang NH, Blough MD, Chesnelong C, Kelly JJ, et al. An in vivo patient-derived model of endogenous IDH1-mutant glioma. Neuro Oncol 2012;14(2):184–91 doi 10.1093/neuonc/nor207. [PubMed: 22166263]
22. Wakimoto H, Kesari S, Farrell CJ, Curry WT, Jr., Zaupa C, Aghi M, et al. Human glioblastoma-derived cancer stem cells: establishment of invasive glioma models and treatment with oncolytic herpes simplex virus vectors. Cancer Res 2009;69(8):3472–81 doi 10.1158/0008-5472.CAN-08-3886. [PubMed: 19351838]
23. Singh SK, Hawkins C, Clarke ID, Squire JA, Bayani J, Hide T, et al. Identification of human brain tumour initiating cells. Nature 2004;432(7015):396–401 doi 10.1038/nature03128. [PubMed: 15549107]
24. Wakimoto H, Mohapatra G, Kanai R, Curry WT, Jr., Yip S, Nitta M, et al. Maintenance of primary tumor phenotype and genotype in glioblastoma stem cells. Neuro Oncol 2012;14(2):132–44 doi 10.1093/neuonc/nor195. [PubMed: 22067563]
25. Wakimoto H, Tanaka S, Curry WT, Loebel F, Zhao D, Tateishi K, et al. Targetable signaling pathway mutations are associated with malignant phenotype in IDH-mutant gliomas. Clin Cancer Res 2014;20(11):2898–909 doi 10.1158/1078-0432.CCR-13-3052. [PubMed: 24714777]
26. Navis AC, Niclou SP, Fack F, Stieber D, van Lith S, Verrijp K, et al. Increased mitochondrial activity in a novel IDH1-R132H mutant human oligodendroglioma xenograft model: in situ

detection of 2-HG and alpha-KG. Acta Neuropathol Commun 2013;1:18 doi 10.1186/2051-5960-1-18. [PubMed: 24252742]

27. Klink B, Miletic H, Stieber D, Huszthy PC, Campos Valenzuela JA, Balss J, et al. A novel, diffusely infiltrative xenograft model of human anaplastic oligodendroglioma with mutations in FUBP1, CIC, and IDH1. PLoS One 2013;8(3):e59773 doi 10.1371/journal.pone.0059773. [PubMed: 23527265]
28. Tateishi K, Iafrate AJ, Ho Q, Curry WT, Batchelor TT, Flaherty KT, et al. Myc-Driven Glycolysis Is a Therapeutic Target in Glioblastoma. Clin Cancer Res 2016;22(17):4452–65 doi 10.1158/1078-0432.CCR-15-2274. [PubMed: 27076630]
29. Tateishi K, Tateishi U, Nakanowatari S, Ohtake M, Minamimoto R, Suenaga J, et al. (62)Cu-diacetyl-bis (N(4)-methylthiosemicarbazone) PET in human gliomas: comparative study with [(18)F]fluorodeoxyglucose and L-methyl-[(11)C]methionine PET. AJNR Am J Neuroradiol 2014;35(2):278–84 doi 10.3174/ajnr.A3679. [PubMed: 23928140]
30. Tripathi M, Sharma R, Varshney R, Jaimini A, Jain J, Souza MM, et al. Comparison of F-18 FDG and C-11 methionine PET/CT for the evaluation of recurrent primary brain tumors. Clin Nucl Med 2012;37(2):158–63 doi 10.1097/RLU.0b013e318238f51a. [PubMed: 22228339]
31. Hunter C, Smith R, Cahill DP, Stephens P, Stevens C, Teague J, et al. A hypermutation phenotype and somatic MSH6 mutations in recurrent human malignant gliomas after alkylator chemotherapy. Cancer Res 2006;66(8):3987–91 doi 10.1158/0008-5472.CAN-06-0127. [PubMed: 16618716]
32. van Thuijl HF, Mazor T, Johnson BE, Fouse SD, Aihara K, Hong C, et al. Evolution of DNA repair defects during malignant progression of low-grade gliomas after temozolomide treatment. Acta Neuropathol 2015;129(4):597–607 doi 10.1007/s00401-015-1403-6. [PubMed: 25724300]
33. Zhang Y, Kwok-Shing Ng P, Kucherlapati M, Chen F, Liu Y, Tsang YH, et al. A Pan-Cancer Proteogenomic Atlas of PI3K/AKT/mTOR Pathway Alterations. Cancer Cell 2017;31(6):820–32 e3 doi 10.1016/j.ccell.2017.04.013. [PubMed: 28528867]
34. Kang S, Bader AG, Vogt PK. Phosphatidylinositol 3-kinase mutations identified in human cancer are oncogenic. Proc Natl Acad Sci U S A 2005;102(3):802–7 doi 10.1073/pnas.0408864102. [PubMed: 15647370]
35. Tateishi K, Higuchi F, Miller JJ, Koerner MVA, Lelic N, Shankar GM, et al. The Alkylating Chemotherapeutic Temozolomide Induces Metabolic Stress in IDH1-Mutant Cancers and Potentiates NAD+ Depletion-Mediated Cytotoxicity. Cancer Res 2017;77(15):4102–15 doi 10.1158/0008-5472.CAN-16-2263. [PubMed: 28625978]
36. Yip S, Miao J, Cahill DP, Iafrate AJ, Aldape K, Nutt CL, et al. MSH6 mutations arise in glioblastomas during temozolomide therapy and mediate temozolomide resistance. Clin Cancer Res 2009;15(14):4622–9 doi 10.1158/1078-0432.CCR-08-3012. [PubMed: 19584161]
37. Choi S, Yu Y, Grimmer MR, Wahl M, Chang SM, Costello JF. Temozolomide-associated hypermutation in gliomas. Neuro Oncol 2018;20(10):1300–9 doi 10.1093/neuonc/noy016. [PubMed: 29452419]
38. Shankar GM, Kirtane AR, Miller JJ, Mazdiyasni H, Rogner J, Tai T, et al. Genotype-targeted local therapy of glioma. Proc Natl Acad Sci U S A 2018;115(36):E8388–E94 doi 10.1073/pnas.1805751115. [PubMed: 30082399]
39. Aihara K, Mukasa A, Nagae G, Nomura M, Yamamoto S, Ueda H, et al. Genetic and epigenetic stability of oligodendrogliomas at recurrence. Acta Neuropathol Commun 2017;5(1):18 doi 10.1186/s40478-017-0422-z. [PubMed: 28270234]
40. Bardella C, Al-Dalahmah O, Krell D, Brazauskas P, Al-Qahtani K, Tomkova M, et al. Expression of Idh1(R132H) in the Murine Subventricular Zone Stem Cell Niche Recapitulates Features of Early Gliomagenesis. Cancer Cell 2016;30(4):578–94 doi 10.1016/j.ccell.2016.08.017. [PubMed: 27693047]
41. Philip B, Yu DX, Silvis MR, Shin CH, Robinson JP, Robinson GL, et al. Mutant IDH1 Promotes Glioma Formation In Vivo. Cell Rep 2018;23(5):1553–64 doi 10.1016/j.celrep.2018.03.133. [PubMed: 29719265]
42. McNeill RS, Stroobant EE, Smithberger E, Canoutas DA, Butler MK, Shelton AK, et al. PIK3CA missense mutations promote glioblastoma pathogenesis, but do not enhance targeted PI3K

inhibition. PLoS One 2018;13(7):e0200014 doi 10.1371/journal.pone.0200014. [PubMed: 29975751]

Translational Relevance

Oligodendroglial tumors (ODs) comprise a relatively indolent subtype of adult diffuse gliomas, however, the majority of ODs eventually develop outgrowth of a subclone that has undergone malignant transformation. Modeling the molecular mechanisms of OD tumor progression is crucial to identify therapeutic targets for malignant disease. Here, we present novel patient-derived anaplastic oligodendroglioma (AOD) orthotopic xenograft models. We established 6 OD intracerebral xenograft models, all of which were found to harbor PI3K/AKT/mTOR pathway gene activating mutations, including *PIK3CA* at E542K and H1047L hotspot mutations. In contrast, OD/AOD tumors that did not form xenograft did not have detectable activation of the PI3K/AKT/mTOR pathway. Importantly, we found progressive tumor cells with mutant *PIK3CA* were vulnerable to alkylating agents and PI3K/AKT/mTOR pathway inhibitors *in vitro* and *in vivo*. These findings suggest a critical role of PI3K/AKT/mTOR pathway activation in driving progression and xenograft formation in ODs and identify potential therapeutic strategies for progressive tumors.

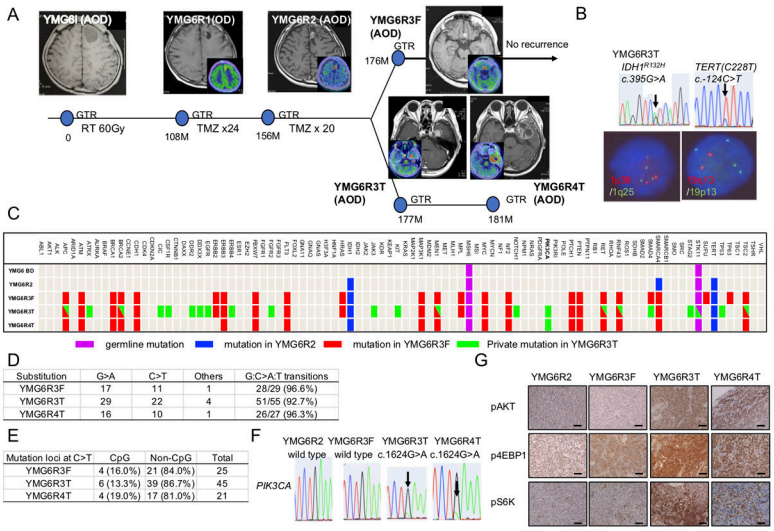

Figure 1: Clinical, pathological, and genomic characteristics of the patient YMG6.

A, Clinical course of anaplastic oligodendroglioma YMG6 with brain MRI and ^{11}C-methionine PET images. YMG6I (treatment naïve), YMG6R1(OD, 1st relapse, ^{11}C-methionine PET; SUVmax =2.6, tumor to normal ratio (T/N)=1.4)), YMG6R2 (AOD, 2nd relapse, SUVmax = 5.6, T/N=4.8), YMG6R3F (3rd relapse at frontal lobe, SUVmax = 5.3, T/N=3.1), YMG6R3T (3rd relapse at temporal lobe, SUVmax =6.6, T/N=4.3), YMG6R4T (4th relapse, SUVmax =6.9, T/N=3.5). GTR, gross total resection. RT, radiation therapy. TMZ, temozolomide. **B**, Genetic analysis of YMG6R3T. Upper: Sanger sequencing for *IDH1* (arrow, c.395G>A) and TERT (arrow, c.−124C>T, C228T). Lower: left, fluorescence in situ hybridization (FISH) for 1p36 (red) and 1q25 (green). Right, FISH for 19q13 (red) and 19p13 (green). **C**, Multiplex PCR based MGH SNaPshot assay and Sanger Sequencing identifying mutations in blood (YMG6 BD), YMG6R2, YMG6R3F, YMG6R3T, and YMG6R4T DNA. **D**, **E**, Frequencies of G:C>A:T transitions (**D**) and C>T change at CpG or non-CpG sites (**E**) in YMG6R3F, YMG6R3T, and YMG6R4T. **F**, Sanger sequencing showing *PIK3CA* mutation (arrows, E542K) in YMG6R3T and YMG6R4T and not in YMG6R2 and YMG6R3F. **G**, Immunohistochemistry for phospho-AKT (Ser473, upper), phospho-S6K (middle), and phospho-4EBP1 (lower) in YMG6R2, YMG6R3F, YMG6R3T, and YMG6R4T. Bars, 50 μm.

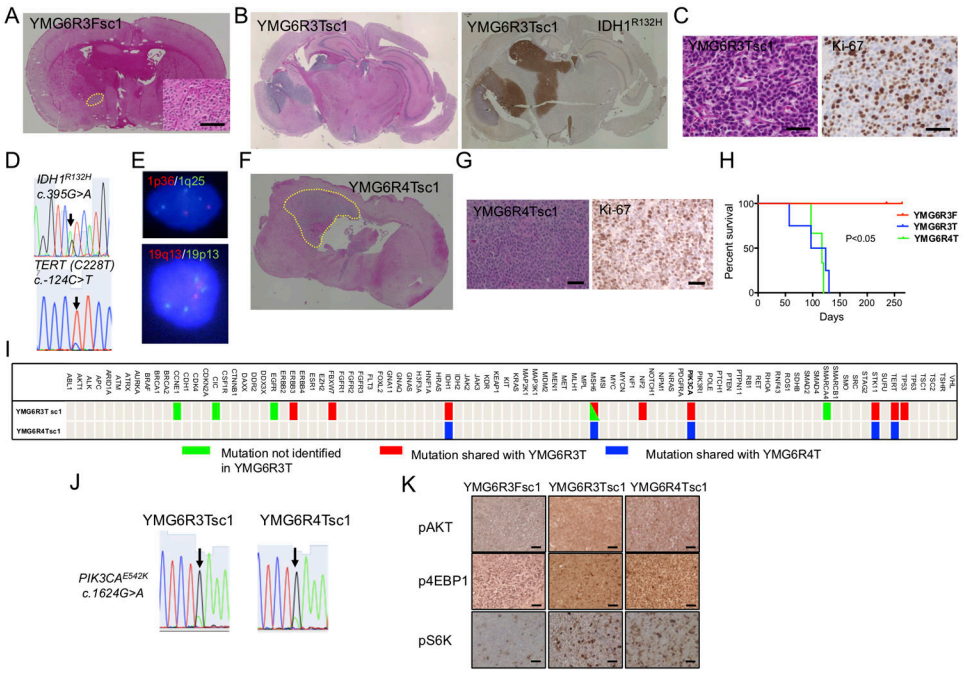

Figure 2: PIK3CA mutant patient-derived anaplastic oligodendroglioma orthotopic xenograft models recapitulating the phenotypic and genotypic characteristics of the patient.

A, Hematoxylin and eosin (H&E) staining of YMG6R3F xenograft (YMG6R3Fsc1, left; overview with the tumor indicated by yellow dotted line, right; microscopic view). **B**, Overview: H&E (left) and IDH1^{R132H} (right) staining in YMG6R3T xenograft (YMG6R3Tsc1). **C**, H&E (left) and Ki-67 (right) staining in YMG6R3Tsc1. **D**. Sanger sequencing for *IDH1* (arrow, c.395 G>A, upper) and *TERT* (arrow, c.−124 C>T, C228T, lower) in YMG6R3Tsc1. **E**, FISH for 1p36 (red) and 1q25 (green, upper), 19q13 (red) and 19p13 (green, lower). **F,** Overview of H&E stained YMG6R4T orthotopic xenograft. The tumor is indicated by yellow dotted line **G**, H&E (left) and Ki-67 (right) staining in YMG6R4T xenograft (YMG6R4Tsc1). **H**, Kaplan-Meier curves demonstrating survival differences between YMG6R3F (red line), YMG6R3T (blue line), and YMG6R4T (green line) implanted mice. **I,** Multiplex PCR based MGH SNaPshot assay identifying mutations in YMG6R3T xenograft (YMG6R3Tsc1) and YMG6R4T xenograft (YMG6R4Tsc1). Green bars; mutations not identified in YMG6R3T. Red bars; shared mutations with YMG6R3T. Blue bars; shared mutations with YMG6R4T. **J**, Sanger sequencing of *PIK3CA* (arrow, c. 1624G>A, E542K) in YMG6R3Tsc1 and YMG6R4Tsc1. **K**, Immunohistochemistry for phospho-AKT (upper), phospho-4EBP1 (middle), and phospho-S6K (lower) in YMG6R3Fsc1, YMG6R3Tsc1, and YMG6R4Tsc1 xenograft tumors. Bars, 50 μm.

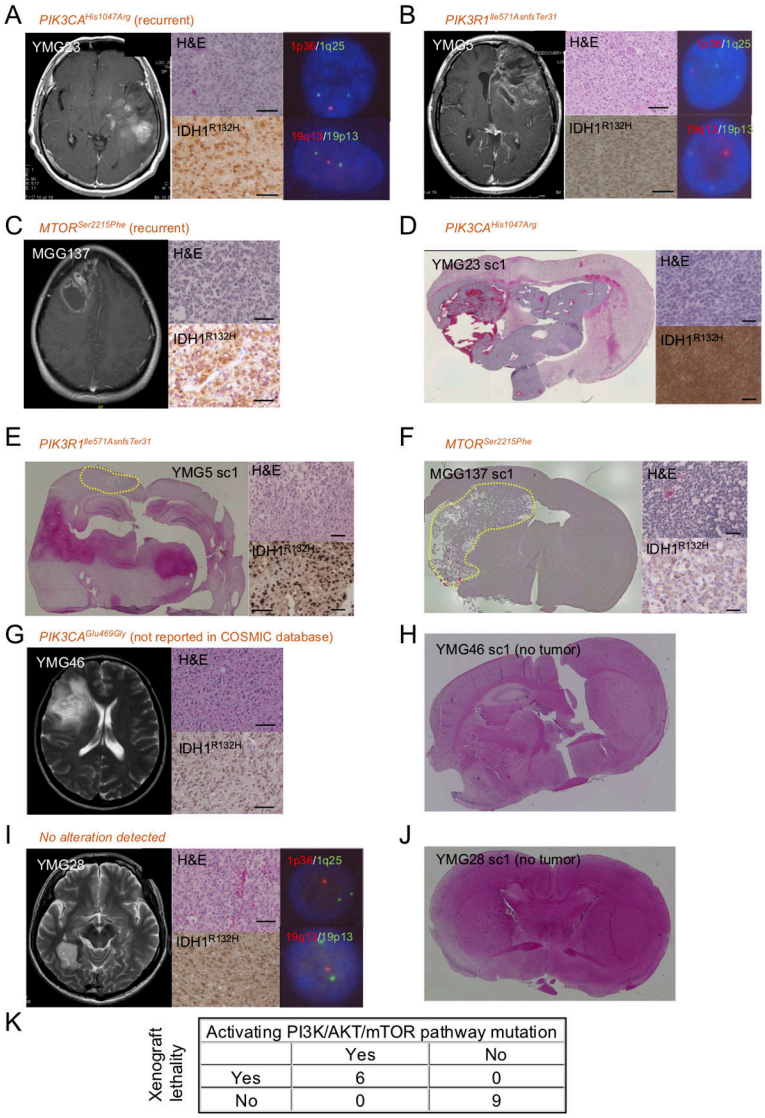

Figure 3: PI3K/AKT/mTOR pathway gene alteration is associated with OD xenograft generation.

A-C, Contrast enhancing T1 weighted MR images, H&E staining and IDH1^{R132H} immunohistochemistry of patient tumors. **A**, YMG23 carrying *IDH1*^{Arg132His}, *TERT (C228T)*, *DDX3X*^{Arg503Gly}, *TP53*^{Glu11Gln}, and *PIK3CA*^{His1047Arg}. **B**, YMG5 carrying *IDH1*^{Arg132His}, *TERT (C228T)*, *DDX3X*^{Arg351Trp}, *HNF1A*$^{c.711T>C}$, and *PIK3R1*^{Ile57AsnfsTer31}. **C**, MGG137 harboring *IDH1*^{Arg132His}, *TERT (C228T)*, and *mTOR*^{Ser2215Phe}. **D-F**, H&E staining and IDH1^{R132H} immunohistochemistry of xenografts. **D,** YMG23 xenograft model (sc1). **E**, YMG5 xenograft model (sc1). **F**, MGG137 xenograft model (sc1). Left, H&E staining (overview). Right, H&E (upper) and IDH1^{R132H} (lower). Tumor is indicated by yellow dotted line. **G**, YMG46 carrying *IDH1*^{Arg132His}, *TERT (C228T), and PIK3CA*^{Glu469Gly}. **H**, H&E stained brain section derived from YMG46 implanted mouse. **I**, YMG28 harboring *IDH1*^{Arg132His}, *TERT (C228T)*, and *CIC splice acceptor variant*. **J**, H&E stained brain section derived from YMG28 implanted mouse. Bars,

50 μm. **K**, Number of oligodendroglioma/anaplastic oligodendroglioma cases stratified by PI3K/AKT/mTOR pathway gene alteration and xenograft lethality. FISH for 1p36 (red) and 1q25 (green, right, upper), 19q13 (red) and 19p13 (green, right, lower). **G** and **I**, T2 weighted MRI due to lack of enhancement.

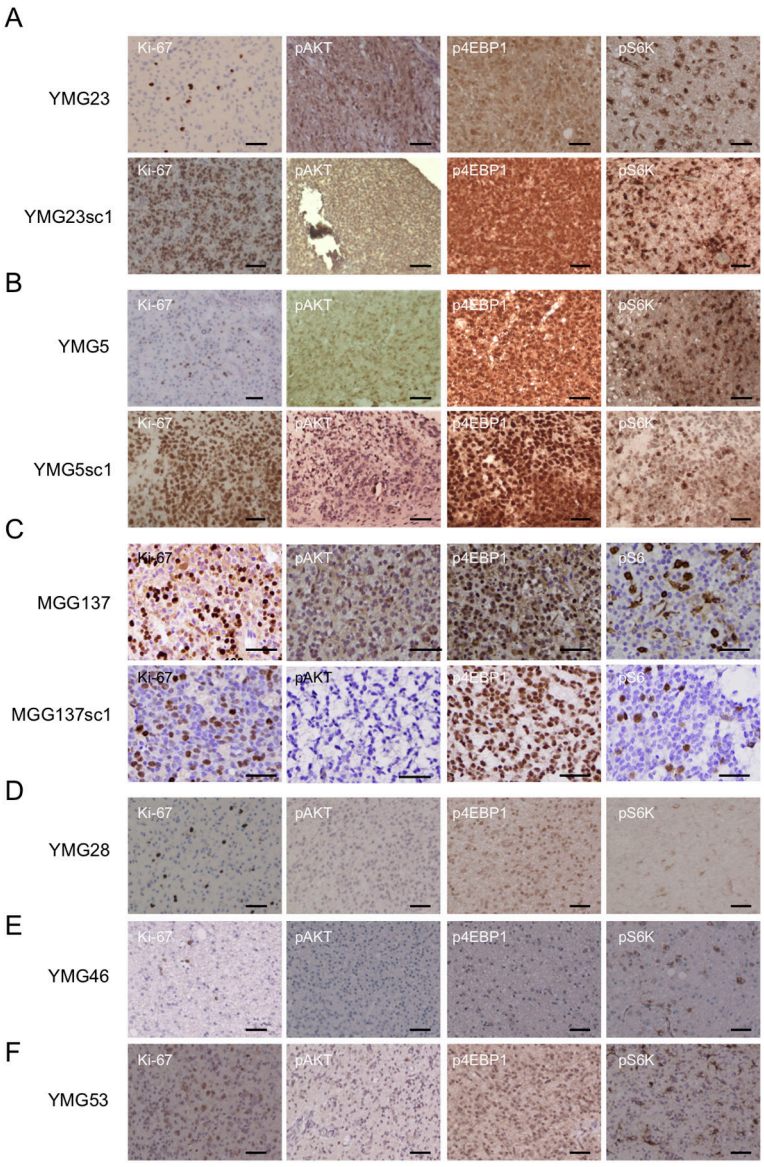

Figure 4. Activation of PI3K/Akt/mTOR signaling in oligodendroglial tumors and xenografts that harbor alteration in PI3K/Akt/mTOR pathway genes.

Immunohistochemical analysis demonstrating Ki-67, p-AKT (Ser473), p-4EBP1, and pS6K expression in xenograft generating oligodendroglial tumors and corresponding xenografts (YMG23 and YMG23sc1 (**A**), YMG5 and YMG5sc1 (**B**), and YMG137 and MGG137sc1 (**C**)), and oligodendroglial tumors that did not generate xenografts (YMG28 (**D**), YMG46 (**E**), and YMG53 (**F**)). Bars, 50um.

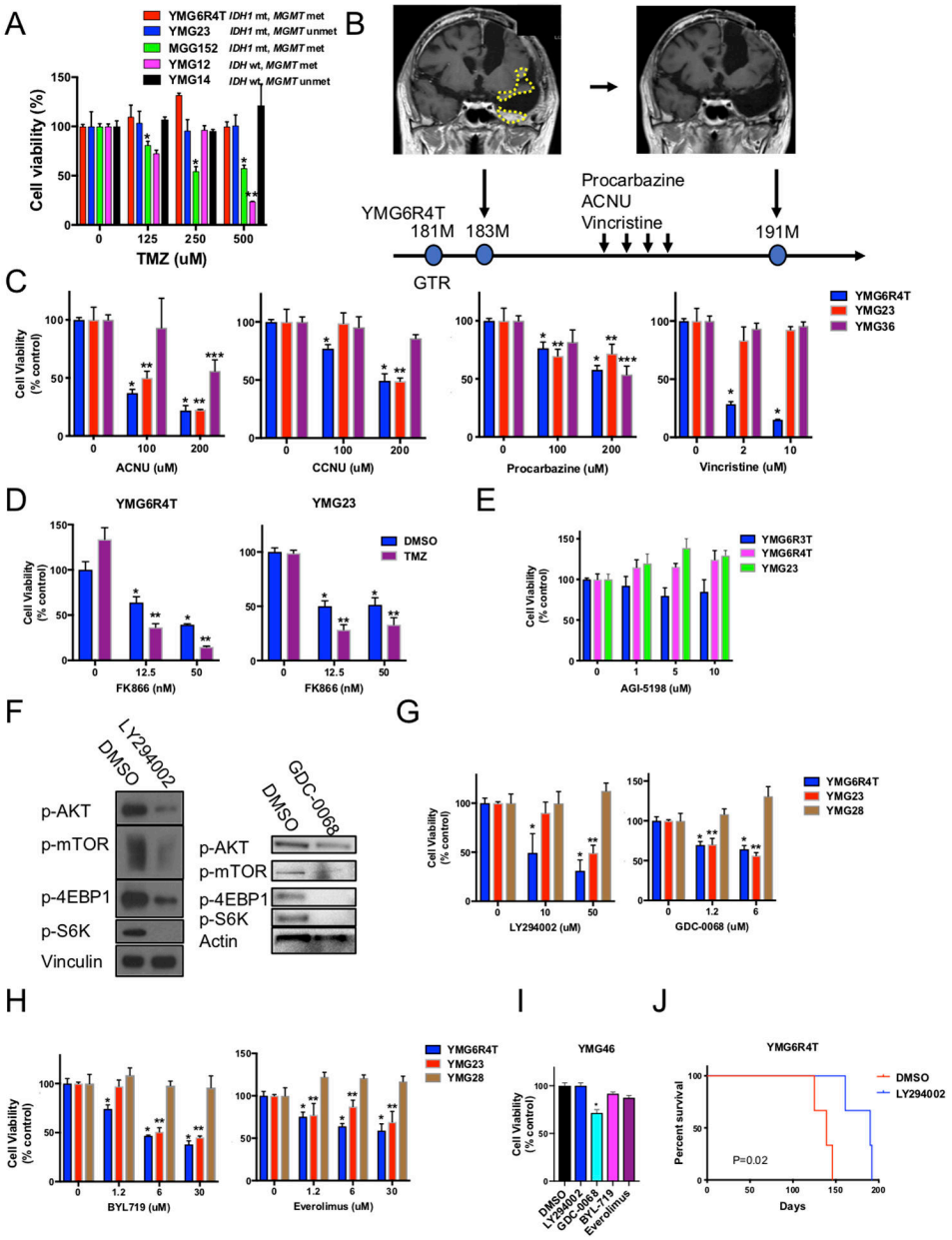

Figure 5: Alkylating chemotherapy and molecular targeted agents target PI3K pathway mutant oligodendroglial tumors.

A, Cell Titer-Glo cell viability assay after 6-day temozolomide treatment for glioma tumorsphere lines. *, ** P<0.05 for the difference between DMSO and TMZ at indicated concentration in MGG152 (*) and YMG12 (**). **B,** Complete remission of recurrent AOD after 4-cycle (8 months) of a chemotherapeutic regimen consisting of procarbazine, nimustine (ACNU), and vincristine. Contrast enhanced MRI showing rapid recurrence (yellow circles) 2 months after gross total resection (GTR) of YMG6R4T (left) and post-chemotherapy (right). **C**, Cell Titer-Glo cell viability assay after 3-day treatment of anaplastic oligodendroglioma lines (YMG6R4T and YMG23, both *PIK3CA* mutant) and a glioblastoma line (YMG36) with ACNU, CCNU, procarbazine, or vincristine. *, **, ***

P<0.05 for the difference between DMSO and indicated chemotherapeutic agent in YMG6R4T (*), YMG23 (**), and YMG36 (***). **D**, Relative cell viability of YMG6R4T (left) and YMG23 (right) cells after 3-day treatment with FK866 combined with DMSO control (blue bars) or TMZ (200 μM, purple bars). *, P<0.05 for difference DMSO and FK866. **, P<0.05 for difference DMSO and FK866 plus TMZ. **E**, Cell viability of YMG6R3T, YMG6R4T and YMG23 cells (all *PIK3CA* mutant) after 9-day exposure with AGI-5198 (IDH1R132H specific inhibitor), relative to DMSO control. **F**, Western blot analysis of p-AKT, p-mTOR, p-4EBP1, and p-S6K expression in YMG6R4T cells after 12 hr-treatment with DMSO control, LY294002 (PI3K inhibitor, 50 μM, left), and GDC-0068 (AKT inhibitor, 5 μM, right). **G**, Cell Titer-Glo cell viability assay after 3-day treatment of YMG6R4T, YMG23, and YMG28 (PI3K pathway gene wild-type) AOD cells with LY294002 or GDC-0068. *, ** P<0.05 for the difference between DMSO and treatment at indicated concentration in YMG6R4T(*) and YMG23 (**). **H**, Cell Titer-Glo cell viability assay after 3-day treatment of YMG6R4T, YMG23, and YMG28 (PI3K pathway gene wild-type) AOD cells with BYL719 (PI3K inhibitor) or everolimus (mTOR inhibitor). *, ** P<0.05 for the difference between DMSO and treatment at indicated concentration in YMG6R4T(*) and YMG23 (**). **I**, Cell Titer-Glo cell viability assay after 3-day treatment of YMG46 (*PIK3CA*^{Glu469Gly}, not reported in COSMIC database) AOD cells with LY294002, GDC-0068, BYL719, or everolimus. * P<0.05 for the difference between DMSO and treatment at indicated concentration. **J**, Kaplan-Meier curves indicating survival difference between mice implanted with DMSO (24hr, n=3) or LY294002 (50 μM, 24hr, n=3) pretreated YMG6R4Tsc2 cells (2×10^5 cells/mouse). Bars, SEM.

Table 1

Characteristics of oligodendroglial tumors used in xenograft assays

Cell line	Histology	Xenograft-induced lethality	Mutation in PI3K/Akt/mTOR pathway
YMG5	AOD	Yes	PIK3R1 I571NfsTer31
YMG6R3T	AOD	Yes	PIK3CA E542K
YMG6R4T	AOD	Yes	PIK3CA E542K
YMG23	AOD	Yes	PIK3CA H1047R
MGG60	AOD	Yes	PIK3CA H1047L
MGG137	AOD	Yes	mTOR S2215F
YMG6R3F	AOD	No	None
YMG28	AOD	No	None
YMG46	OD	No	PIK3CA E469G
YMG53	AOD	No	None
MGG78	OD	No	None
MGG82	AOD	No	None
MGG109	AOD	No	None
MGG126	AOD	No	None
MGG130	AOD	No	None